Original Article

ADK-VR2, a cell line derived from a treatment-naïve patient with *SDC4-ROS1* fusion-positive primarily crizotinib-resistant NSCLC: a novel preclinical model for new drug development of ROS1-rearranged NSCLC

Francesca Ruzzi[1#], Stefania Angelicola[1#], Lorena Landuzzi[2#], Elena Nironi[1], Maria Sofia Semprini[1], Laura Scalambra[1], Annalisa Altimari[3], Elisa Gruppioni[3], Michelangelo Fiorentino[4], Francesca Giunchi[3], Manuela Ferracin[4], Annalisa Astolfi[4], Valentina Indio[5], Andrea Ardizzoni[4,6], Francesco Gelsomino[4,6], Patrizia Nanni[1,7], Pier-Luigi Lollini[1,7*], Arianna Palladini[8,9*^]

[1]Laboratory of Immunology and Biology of Metastasis, Department of Experimental, Diagnostic and Specialty Medicine (DIMES), University of Bologna, Bologna, Italy; [2]Laboratory of Experimental Oncology, IRCCS Istituto Ortopedico Rizzoli, Bologna, Italy; [3]Divisione di Anatomia Patologica, IRCCS Azienda Ospedaliero-Universitaria di Bologna, Bologna, Italy; [4]Department of Experimental, Diagnostic and Specialty Medicine (DIMES), University of Bologna, Bologna, Italy; [5]Department of Veterinary Medical Sciences, University of Bologna, Bologna, Italy; [6]Divisione di Oncologia Medica, IRCCS Azienda Ospedaliero-Universitaria di Bologna, Bologna, Italy; [7]Alma Mater Institute on Healthy Planet, University of Bologna, Bologna, Italy; [8]Department of Pharmacy and Biotechnology, University of Bologna, Bologna, Italy; [9]Department of Molecular Medicine, University of Pavia, Pavia, Italy

Contributions: (I) Conception and design: F Ruzzi, S Angelicola, F Gelsomino, PL Lollini, A Palladini; (II) Administrative support: F Ruzzi, A Palladini; (III) Provision of study materials or patients: F Gelsomino, A Ardizzoni; (IV) Collection and assembly of data: All authors; (V) Data analysis and interpretation: A Palladini, S Angelicola, F Ruzzi; (VI) Manuscript writing: All authors; (VII) Final approval of manuscript: All authors.

[#]These authors contributed equally to this work.

[*]These authors jointly supervised this work.

Correspondence to: Arianna Palladini, PhD. Department of Molecular Medicine, University of Pavia, Via Ferrata 9, 27100 Pavia, Italy. Email: arianna.palladini@unipv.it; Francesco Gelsomino, MD. Divisione di Oncologia Medica, IRCCS Azienda Ospedaliero-Universitaria di Bologna, via Albertoni 2, 40138 Bologna, Italy. Email: francesco_gelsomino@aosp.bo.it.

Background: ROS1 fusions are driver molecular alterations in 1–2% of non-small cell lung cancers (NSCLCs). Several tyrosine kinase inhibitors (TKIs) have shown high efficacy in patients whose tumors harbour a ROS1 fusion. However, the limited availability of preclinical models of ROS1-positive NSCLC hinders the discovery of new drugs and the understanding of the mechanisms underlying drug resistance and strategies to overcome it.

Methods: The ADK-VR2 cell line was derived from the pleural effusion of a treatment-naïve NSCLC patient bearing *SDC4-ROS1* gene fusion. The sensitivity of ADK-VR2 and its crizotinib-resistant clone ADK-VR2 AG143 (selected in 3D culture in the presence of crizotinib) to different TKIs was tested *in vitro*, in both 2D and 3D conditions. Tumorigenic and metastatic ability was assessed in highly immunodeficient mice. In addition, crizotinib efficacy on ADK-VR2 was evaluated *in vivo*.

Results: 2D-growth of ADK-VR2 cells was partially inhibited by crizotinib. On the contrary, the treatment with other TKIs, such as lorlatinib, entrectinib and DS-6051b, did not result in cell growth inhibition. TKIs showed dramatically different efficacy on ADK-VR2 cells, depending on the cell culture conditions. In 3D culture, ADK-VR2 growth was indeed almost totally inhibited by lorlatinib and DS-6051b. The clone ADK-VR2 AG143 showed higher resistance to crizotinib treatment *in vitro*, compared to its parental cell line, in both 2D and 3D cultures. Similarly to ADK-VR2, ADK-VR2 AG143 growth was strongly inhibited by

^ ORCID: 0000-0001-6105-4895.

lorlatinib in 3D conditions. Nevertheless, ADK-VR2 AG143 sphere formation was less affected by TKIs treatment, compared to the parental cell line. *In vivo* experiments highlighted the high tumorigenic and metastatic ability of ADK-VR2 cell line, which, once injected in immunodeficient mice, gave rise to both spontaneous and experimental lung metastases while the crizotinib-resistant clone ADK-VR2 AG143 showed a slower growth *in vivo*. In addition, ADK-VR2 tumor growth was significantly reduced but not eradicated by crizotinib treatment.

Conclusions: The ADK-VR2 cell line is a promising NSCLC preclinical model for the study of novel targeted therapies against ROS1 fusions and the mechanisms of resistance to TKI therapies.

Keywords: Non-small cell lung cancer (NSCLC); ROS1 fusion; tyrosine kinase inhibitors (TKIs); target therapies; receptor tyrosine kinase (RTK)

Submitted Mar 02, 2022. Accepted for publication Sep 12, 2022.
doi: 10.21037/tlcr-22-163
View this article at: https://dx.doi.org/10.21037/tlcr-22-163

Introduction

Non-small cell lung cancer (NSCLC) is a heterogeneous disease in which the discovery of several molecular driver alterations has led to the development of targeted drugs that have dramatically improved the survival of patients with oncogene-addicted NSCLC (1). Beyond the most common activating *EGFR* and *KRAS* (p.G12C) mutations, *ALK* and *ROS1* gene rearrangements, accounting for 5–7% and 1–2% of all NSCLC cases respectively, confer a highly aggressive behaviour on tumor cells and need specific therapeutic approaches (2,3).

ROS1 is a proto-oncogene involved in cell growth, differentiation and survival. The gene is homologous to the *v-ros* sequence of the avian sarcoma virus UR2 and encodes a receptor tyrosine kinase (RTK), which is structurally characterized by a large extracellular N-domain including sequences that can play a role in cell adhesion, and a C-terminal portion whose sequence is most closely related to the ALK human RTK (3,4). Despite this knowledge, the physiological role of ROS1 in humans remains unknown, and no ROS1 ligand has been so far identified, except for neural epidermal growth factor-like 2 (NELL2) in mice. The specific role of this protein in human ROS1 activation has to be still investigated (3,5).

Fusions of ROS1 intracellular kinase domain to the N-terminal domain of a partner gene have been reported in several tumor types, including carcinomas and sarcomas. In most cases the result of these fusions is the constitutive activation of ROS1 kinase, triggering cell survival and growth signalling pathways (3,6,7).

About 26 genes have been found to be possible partners for ROS1 fusion (8-10). Although *CD74-ROS1* is the most common ROS1 fusion in NSCLC (44%), *SDC4-ROS1* was also found in 14% of patients with ROS1-rearranged NSCLCs, as well as *EZR-ROS1* in 16% of patients (3). ROS1-positive NSCLC patients usually show high sensitivity to pemetrexed-based chemotherapy (11-13). Nevertheless, the impressive results of crizotinib, a multi-targeted (MET/ALK/ROS1) tyrosine kinase inhibitor (TKI), led to its approval for the treatment of advanced ROS1-rearranged NSCLC patients by US and European regulatory medicinal agencies (FDA and EMA) in 2016 (14). Afterwards, second generation ALK and ROS1 TKIs, including lorlatinib and entrectinib, have also been recently approved for clinical use in ROS1-rearranged NSCLC patients (15). Nevertheless, the limited number of preclinical models of ROS1-altered NSCLC makes it difficult to compare the activity of different TKIs on different ROS1 fusions (3).

In this paper, we report a new NSCLC cell line, namely ADK-VR2, obtained from the pleural effusion of a treatment-naïve patient with *SDC4-ROS1*-positive NSCLC. Cells were treated *in vitro* with pemetrexed and several TKIs, providing a wide profile of targeted drug sensitivity. Moreover, *in vivo* studies revealed ADK-VR2 tumorigenic and metastatic abilities. Based on our investigations, we introduce ADK-VR2 cell line as an attractive preclinical model of NSCLC to investigate the sensitivity of new ROS1-targeted drugs, in both *in vitro* and *in vivo* systems. We present the following article in accordance with the ARRIVE reporting checklist (available at https://tlcr.amegroups.com/article/view/10.21037/tlcr-22-163/rc).

Methods

Mice

NOD-SCID-Il2rg$^{-/-}$ (NSG) immunodeficient mice (breeders received from Charles River Laboratories) and BALB/c *Rag2*$^{-/-}$;*Il2rg*$^{-/-}$ (BRG) mice (breeders kindly provided by the Central Institute for Experimental Animals, Kawasaki, Japan) (16) were bred under sterile condition in our animal facilities.

All animal procedures were performed in accordance with European directive 2010/63/UE and Italian Law (No. DL26/2014); experimental protocols were reviewed and approved by the institutional animal care and use committee of the University of Bologna and by the Italian Ministry of Health with letter 32/2020-PR.

Cell lines

ADK-VR2 cell line was derived from the pleural effusion of a treatment-naïve patient with *SDC4-ROS1* positive NSCLC, who later resulted to be primarily resistant to crizotinib (Xalkori, Pfizer). The study was conducted in accordance with the Declaration of Helsinki (as revised in 2013). Human samples were collected after patient gave his informed consent. The protocol was approved by the Ethics Committee Center Emilia-Romagna Region, Italy (protocol 130/2016/U/Tess). Human samples and metadata including relevant clinical data were de-identified before being shared between laboratories involved in this study. A primary cell culture was established from the sample: the pleural effusion was centrifugated at 250 g for 5 minutes and cell sediment was then seeded in a 25 cm^2 PRIMARIA tissue culture flask (Corning). Cells were cultured in MammoCult medium (STEMCELL Technologies, Vancouver, Canada) supplemented with 1% fetal bovine serum (FBS; Thermo Fisher Scientific, Monza, Italy), 100 U/mL penicillin and 10 µg/mL streptomycin (Thermo Fisher Scientific) and grown at 37 ℃ in a humidified atmosphere at 5% CO_2.

ADK-VR2 AG143 is a clone of ADK-VR2 cell line isolated from a 3D culture in the presence of crizotinib 0.02 µM for three weeks (Merck Life Science, Milan, Italy). The clone was cultured and grown under the same conditions described above.

HCC-78 cell line was a kind gift by Prof. Manuela Iezzi (G. D'Annunzio University, Chieti, Italy). Cells were cultured in RPMI medium (Thermo Fisher Scientific) supplemented with 10% FBS, 100 U/mL penicillin and 10 µg/mL streptomycin and grown at 37 ℃ in a humidified atmosphere at 5% CO_2.

Molecular analysis

Total RNA was extracted from cell pellets using Trizol Reagent (Thermo Fisher Scientific), according to the manufacturer's instructions. DNA was extracted using a PureLink Genomic DNA Mini kit (Thermo Fisher Scientific), according to the manufacturer's protocol.

Molecular analysis to detect *EGFR* and *KRAS* mutations was performed on cell blocks obtained from pleural effusion by real time (RT)-polymerase chain reaction (PCR) (TheraScreen-Qiagen, Milan, Italy). Immunohistochemistry was performed on the formalin-fixed, paraffin-embedded sections of liver biopsy using the following pre-diluited antibodies: PDL1 (clone SP263 Ventana, Roche, Monza, Italy), ALK (clone D5F3, Ventana), and TTF1 (Clone 8G7G3/1, Ventana), Ep-CAM/Epithelial Specific Antigen (clone BerEP4, Ventana), calretinin (clone SP85, Ventana). Hematoxylin and eosin (H&E) staining was also performed on the specimens. Gene rearrangement was evaluated by fluorescence in situ hybridization (FISH). FISH assay was performed using the Zytolight SPEC ROS1 Dual Color Break Apart Probe (ZytoVision, Germany).

For whole transcriptome sequencing (WTS), cDNA libraries were synthesized from 500 ng total RNA using the TruSeq Stranded mRNA kit (Illumina), following manufacturer's instructions. For whole exome sequencing (WES), libraries were synthesized with Nextera Rapid Capture Exome Kit (Illumina) from the cell line and patients' peripheral blood following the manufacturer's recommendations.

A detailed description of performed molecular analyses was reported in Appendix 1.

Drug sensitivity in 2D culture condition

ADK-VR2, HCC-78 and ADK-VR2 AG143 cell lines, within 30th *in vitro* passage, were seeded at 0.05×10^6 cells (or 0.1×10^6 cells for pemetrexed experiments) per well into 24-well plate in MammoCult + 1% FBS (ADK-VR2 and ADK-VR2 AG143) or RPMI + 10% FBS (HCC-78). After 24 hours from seeding, cells were treated with pemetrexed, crizotinib, lorlatinib, entrectinib or DS-6051b (Merck Life Science; Selleck Chemicals, Houston, TX, USA) by adding 100 µL of a 10× solution of each drug or vehicle (DMSO, Merck). Drug concentrations were reported in the figures. Cell growth was assessed 72 hours later by vital counting with erythrosine.

Drug sensitivity in 3D culture condition

ADK-VR2, ADK-VR2 AG143 and HCC-78 cells were seeded at 500 cells/well in 24-well plate in semisolid medium—MammoCult + 1% FBS + 0.33% agar (Sea-Plaque Agarose, Lonza, Switzerland), containing crizotinib, lorlatinib, entrectinib or DS-6051b 0.01 µM, with a 0.5% agarose underlay. Colonies (diameter >90 µm) were counted 2–4 weeks later under an inverted microscope in dark-field, as previously described (17,18).

Drug sensitivity in a sphere-formation assay

Cells were seeded at 4,000 cells in 4 mL complete MammoCult medium without serum in 6-well Ultra-Low adherence plate (Corning Life Sciences), according to the MammoCult Human Medium Kit protocol. Drugs and vehicle were added to the medium at different doses. Cells were incubated at 37 ℃ in a humidified 5% CO_2 atmosphere for a week. Spheres, multi-cell structures, with a diameter larger than 90 µm were counted about 7 days after the seeding (19).

Tumorigenicity and metastatic ability

BRG 13–25-week-old male mice were used to evaluate the tumorigenicity of ADK-VR2 cell line and ADK-VR2 AG143 clone. Mice received subcutaneous (*s.c.*) injection of 9×10^6 cells, in a hind leg (n=3). Animals were checked weekly, and tumors were measured with calipers. Tumor volume was calculated as $\pi/6*\left(\sqrt{ab}\right)^3$, in which a = maximal tumor diameter and b = maximal tumor diameter perpendicular to a. Before tumors reached 2.5 cm^3, mice were sacrificed by CO_2 inhalation and cervical dislocation. An accurate necropsy was performed and lungs were collected for molecular detection of metastatic dissemination.

BRG male mice, 19–23-week-old, were used to investigate the metastatic ability of ADK-VR2 cell line by the intravenous injection (*i.v.*) of 0.5×10^6 cells into a caudal vein (n=5). Animals were inspected weekly and euthanized as described above at any initial sign of metastatic growth or 18 weeks after cells injection. At necropsy, lungs were dissected to investigate metastatic dissemination.

Crizotinib therapy

Crizotinib was formulated in 5% DMSO, 30% PEG300 (Merck) and 65% double distilled water. ADK-VR2 cell line was injected subcutaneously at the dose of 10^6 cells in NSG female mice (37-week-old) to assess tumor growth. The animals were randomized into control and treated group. Five mice were enrolled in each test group in order to have an 80% chance of showing, with a 5% significance, a 65% of success in the experimental group. Control group was not treated (n=5), treated mice received crizotinib 50 mg/kg daily *per os* by gavage starting from 12 days after cell injection (5 mice were enrolled but a censored mouse at 6 week from cell injection was not included in tumor growth analysis; n=4). Animals were checked weekly, and tumors were measured with calipers. Tumor volume was calculated as described in the previous section and mice were sacrificed as previously described. Blinding to assess the outcome of *in vivo* experiments was not done. To minimize potential confounders, we used labelled cages. Labels had a different colour for each group.

Metastasis quantification in lungs

Lungs were minced with scissors and passed through a 70 µm cell strainer (Becton Dickinson, Bedford, MA, USA) to obtain a homogeneous cell suspension. Genomic DNA was extracted from cell suspensions and molecular quantification of metastatic load in lungs was performed by RT-PCR with human-specific primers as previously described (20,21). Briefly, genomic DNA was extracted with 10 mM Tris-HCl buffer pH 8.3 containing 50 mM KCl, 2.5 mM $MgCl_2$, 0.01% gelatin, 0.45% Igepal, 0.45% Tween 20 and 120 mg/mL proteinase K (all reagents from Merck) by overnight incubation at 56 ℃ followed by 30 min incubation at 95 ℃ to inactivate the proteinase K. A sequence of the α-satellite region of human chromosome 17 was amplified. RT-PCR was performed using a Thermal Cycler CFX96 real time system C1000 (Bio-Rad, CA, USA). To quantify human cells, a standard curve was constructed by adding scalar amounts of MDA-MB-453 human cells to a constant number of mouse cells. Ct (threshold cycle) values obtained from the experimental samples were interpolated in the standard curve run in each PCR (Bio-Rad CFX Manager). A negative control consisting of only mouse cells was included in each PCR. Ct values higher than Ct of the lowest standard curve point or the negative control were considered as negative (0% of human cells).

Statistical analysis

The significance of differences in growth rate and sensitivity

to drugs was assessed through the two-tailed unpaired Student's *t*-test or *t*-test with Welch's correction, according to assumptions of the tests and the variance between the compared groups. The used test was reported in each figure legend.

Calculations of the IC_{50} (half maximal inhibitory concentration) of the drugs used in this paper were based on the interpolation of the growth percentages with a sigmoid dose-response curve by Prism 5 software (GraphPad software, La Jolla, CA, USA) and IC_{50} Calculator | AAT Bioquest (IC_{50} Calculator | AAT Bioquest). The significance of differences in IC_{50} between different cell lines and different drugs was assessed by calculating the IC_{50} value for each replicate and comparing the values of each group through the Student's *t*-test. Statistical analyses were performed through Prism 5 software.

Results

Patient clinical history and molecular data

A 46-year-old Asian, non-smoker male patient, presented with massive right pleural effusion associated with contralateral mediastinal shift and pulmonary dissemination from lung adenocarcinoma (TTF1 positive, BerEP4 positive, calretinin negative) (Figure S1A,S1B). According to molecular analysis of pleural effusion cells, neither *EGFR* nor *KRAS* gene mutations were detected. Furthermore, the sample was positive for PD-L1 tumor proportion score (TPS) staining (25%) and negative for *ALK* rearrangement. Next generation sequencing (NGS) of pleural effusion samples showed the presence of a *SDC4-ROS1* gene fusion (*Figure 1A*).

After pleural effusion drainage and talc slurry, cisplatin (75 mg/mq) and pemetrexed (500 mg/mq) every 3 weeks were administered as first-line therapy up to four courses, with a good tolerance. Unfortunately, at the time of first tumor assessment, a progressive disease was documented in accordance with Response Evaluation Criteria in Solid Tumors (RECIST) v1.1 criteria (appearance of new lesions at liver, lung, bone and central nervous system) (22). According to chemotherapy-failure and ROS1 status, a second-line therapy with crizotinib 250 mg twice daily was started. Because of central nervous system involvement and the poor penetrance of crizotinib through the blood-brain barrier, gamma-knife radiotherapy was performed on three brain lesions.

After two months of TKI treatment, the patient experienced clinical disease progression with worsening of cough and back pain due to thoracic vertebral collapse. A total-body CT scan showed the onset of pulmonary lymphangitis and peritoneal carcinomatosis associated with liver and bone progression. Because of early disease progression to TKI therapy, the patient underwent a liver biopsy, with the aim of obtaining molecular profiling of the disease. FISH testing confirmed the presence of 5' *ROS1* deletion in 62% of analyzed cells (*Figure 1B*). H&E staining of the biopsy showed an adenocarcinoma with acinar structure, consistent with a recurrence of the primary NSCLC (Figure S1C). This finding was also confirmed by the immunoreactivity of the cancer cells for TTF1 (Figure S1D). Gene rearrangements could not be evaluated in the liver sample because of poor RNA quality. After palliative radiotherapy on thoracic vertebrae, a third-line treatment with lorlatinib as part of a compassionate use program was proposed but could not be administered because of rapid and widespread disease progression and clinical deterioration, which in short time led to patient's death.

Cell line molecular profile

From the treatment-naïve pleural effusion of the patient, we derived a new NSCLC cell line called ADK-VR2. In adherent culture conditions, cells showed a polygonal morphology with transepithelial fluid transport formations also known as dome structures (*Figure 1C,1D*). Immunohistochemical and molecular analyses confirmed that these cells were positive for BerEP4 staining (Figure S1E) and carried the *SDC4-ROS1* fusion. No other alterations included in the Oncomine panel were detected by the NGS analysis. The additional somatic mutations recognized by WES in ADK-VR2 are not considered as pathogenic variants based on the current knowledge (Table S1).

In vitro ADK-VR2 drug sensitivity

In adherent culture conditions, ADK-VR2 cell line showed lower sensitivity to pemetrexed than HCC-78 cell line, which bears the *SLC34A2-ROS1* fusion (IC_{50} 0.0677±0.0130 and 0.0096±0.0009 μM, respectively) (*Figure 2A*). HCC-78 pemetrexed sensitivity was in accordance with previous published data (23). Cell viability of both cell lines was partially inhibited by crizotinib (IC_{50} values are around 0.5 μM) (*Figure 2B* and Table S2). Then, we compared the activity of both crizotinib and new generation ROS1

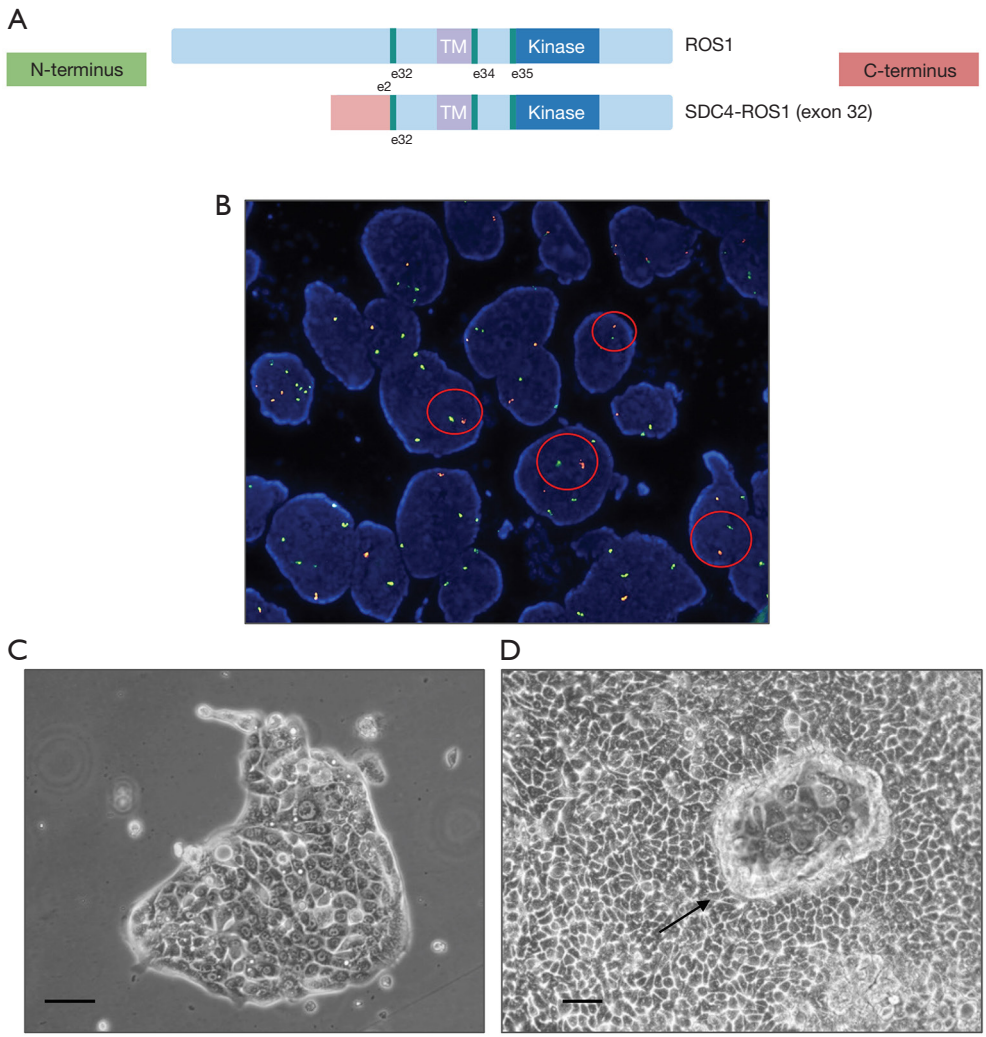

Figure 1 Molecular characterization of patient's tumor samples and morphological characterization of ADK-VR2 cell line. (A) Representative illustration of the *SDC4* (exon 2)-*ROS1* (exon 32) rearrangement. (B) FISH image showing the *ROS1* fusion on liver biopsy. Circled areas represent positive cells to 5' *ROS1* fusion (magnification DAPI ×100). (C) The polygonal morphology of ADK-VR2 cell line in 2D culture (by phase-contrast microscopy). (D) Dome structure by ADK-VR2 cell line (arrow) in 2D culture (by phase-contrast microscopy). Black line corresponds to 100 µm. TM, transmembrane domain; e, exon; FISH, fluorescence in situ hybridization; DAPI, 4',6-diamidino-2-phenylindole blue-fluorescent DNA staining dye.

TKIs against ADK-VR2 and HCC-78 cells. Surprisingly, in adherent culture conditions, ADK-VR2 growth was not inhibited by lorlatinib, entrectinib and DS-6051b (IC_{50} >1 µM, at least) contrary to HCC-78, which showed higher sensitivity to lorlatinib (IC_{50} <0.01 µM), entrectinib (IC_{50} 0.2967±0.1182 µM) and DS-6051b (IC_{50} 0.4309±0.2459 µM) (*Figure 2C* and Table S2). To better elucidate drug activity on ADK-VR2, we employed a 3D-growth in soft-agar assay, and we found that crizotinib and entrectinib activity was significantly higher on ADK-VR2 cells compared to HCC-78 cells (*Figure 2D*). Unexpectedly, lorlatinib and DS-6051b almost completely inhibited ADK-VR2 3D-growth, resulting even more effective than crizotinib in these culture conditions ($P<0.05$ by unpaired *t*-test with Welch's correction). The growth of cells in non-adherent conditions is a label of aggressiveness together with the capability to produce spheres, which is considered as an index of stemness (24,25). The ability of a drug to inhibit stem cell proliferation is a valuable aspect, since cancer stemness is frequently associated with

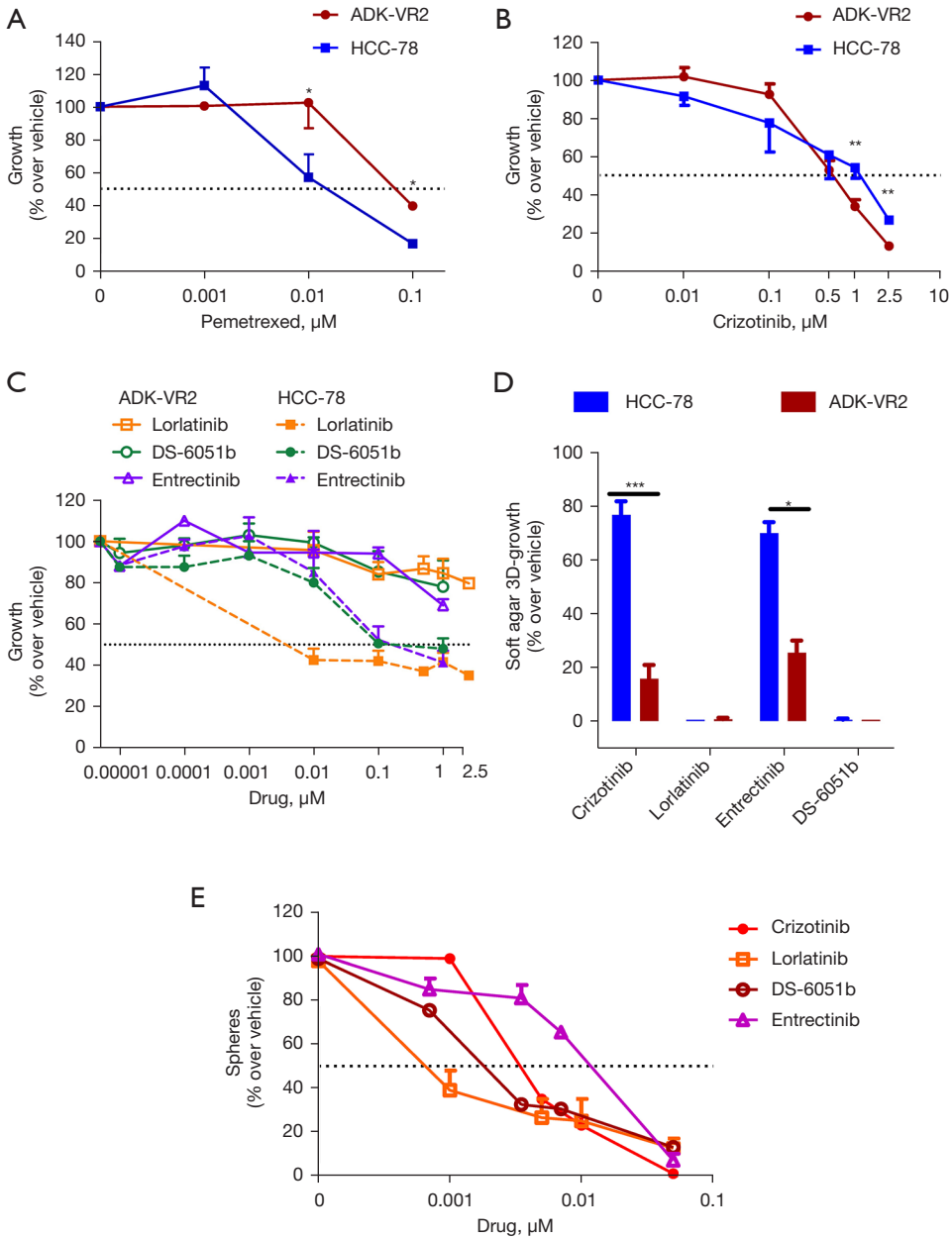

Figure 2 *In vitro* 2D-growth (A-C) and 3D-growth (D,E) drug sensitivity of ADK-VR2 and/or HCC-78 cell lines. (A) ADK-VR2 and HCC-78 sensitivity to pemetrexed (n=2). *, P<0.05 by Student's *t*-test. Each point represents mean and SEM. (B) ADK-VR2 (n=8) and HCC-78 (n=4) sensitivity to crizotinib. **, P<0.01 by Student's *t*-test. Each point represents mean and SEM. (C) ADK-VR2 sensitivity to lorlatinib (n=4), DS-6051b (n=3) and entrectinib (n=2); HCC-78 sensitivity to lorlatinib (n=2), DS-6051b (n=2) and entrectinib (n=3). Each point represents mean and SEM. (D) Soft agar 3D-growth in the presence of crizotinib 0.01 μM (HCC-78, n=4; ADK-VR2, n=6), lorlatinib 0.01 μM (HCC-78, n=2; ADK-VR2, n=4), entrectinib 0.01 μM (HCC-78, n=2; ADK-VR2, n=2) and DS-6051b 0.01 μM (HCC-78, n=2; ADK-VR2, n=2). ***, P<0.001; *, P<0.05 by Student's *t*-test. Each bar represents mean and SEM. (E) ADK-VR2 sphere formation (n=2) in the presence of crizotinib (IC_{50} 0.0040±0.0003 μM), lorlatinib (IC_{50} 0.0003±0.0001 μM), DS-6051b (IC_{50} 0.0013±0.0000 μM) and entrectinib (IC_{50} 0.0233±0.0049 μM). IC_{50} comparison by Student's *t*-test: P<0.01 lorlatinib *vs.* crizotinib and DS-6051b *vs.* crizotinib; P<0.05 lorlatinib *vs.* DS-6051b and entrectinib, DS-6051b *vs.* entrectinib. Each point represents mean and SEM. SEM, standard error of the mean; 2D, two-dimensional; 3D, three-dimensional.

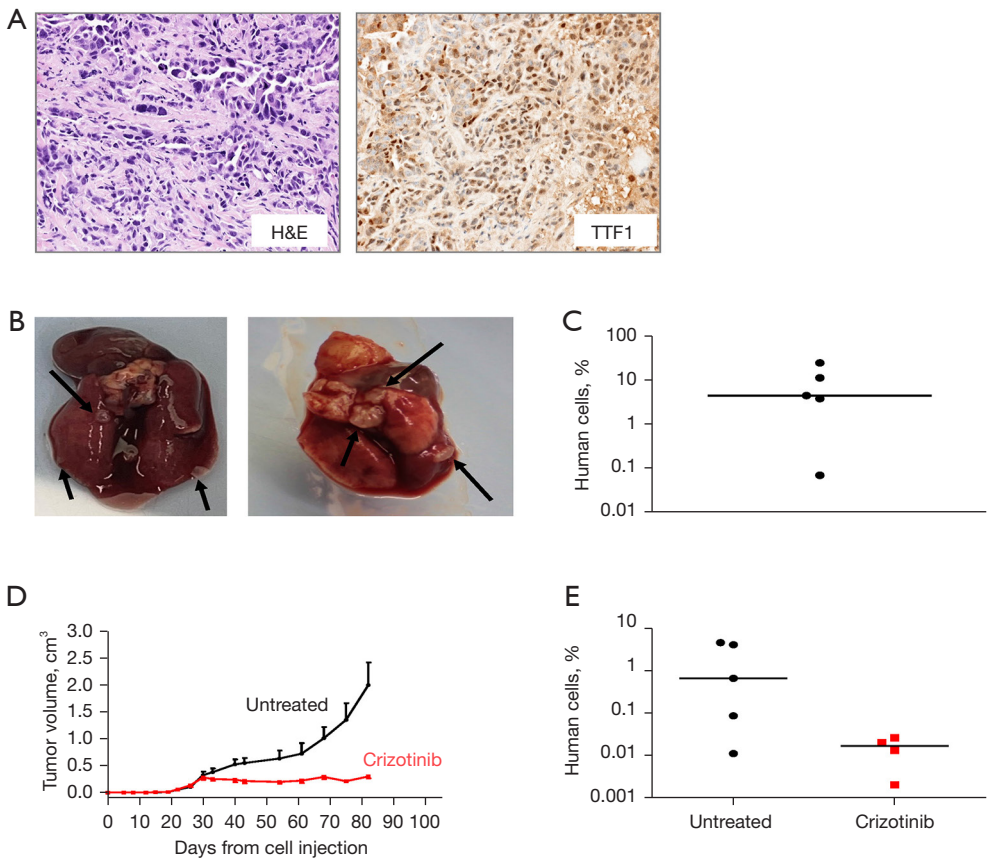

Figure 3 ADK-VR2 *in vivo* growth. (A) Phenotype of a representative tumor induced by *s.c.* injection of ADK-VR2 cells in immunocompromised BRG mice. H&E stain showed a morphology similar to the tumor of patient. TTF1 staining was focal. ×20 magnification. (B) Representative lung pictures of BRG mice receiving *i.v.* injection of ADK-VR2 cells. Arrows indicating some metastatic nodules. (C) Lung metastatic load of BRG mice receiving *i.v.* injection of ADK-VR2 cells quantified by RT-PCR. Horizontal line represents the median. (D) Tumor growth of *s.c.* injected ADK-VR2 cells in NSG mice treated with crizotinib 50 mg/kg *per os*, starting 12 days after cell injection (n=4), or in untreated mice (n=5). Starting from the 40th day after cell injection, P<0.05, at least, by unpaired *t*-test with Welch's correction (except the 61st day, P=0.07). Each point represents mean and SEM. (E) Lung metastatic load of mice described in (D), quantified by RT-PCR. Horizontal line represents the median. H&E, hematoxylin and eosin; *s.c.*, subcutaneous; BRG, BALB/c *Rag2*$^{-/-}$;*Il2rg*$^{-/-}$; *i.v.*, intravenous; NSG, NOD-SCID-*Il2rg*$^{-/-}$; RT-PCR, real time-polymerase chain reaction; SEM, standard error of the mean.

cancer progression, survival and response to treatments (26,27). In this regard, ADK-VR2 sphere production was strongly inhibited by lorlatinib (IC_{50} 0.3 nM), resulting more effective than DS-6051b (IC_{50} 1.3 nM) and crizotinib (IC_{50} 4 nM) in these culture conditions. Entrectinib was effective on sphere formation at a higher concentration (IC_{50} 23.3 nM) (*Figure 2E* and Table S3).

Tumorigenic and metastatic ability and in vivo treatment with crizotinib

ADK-VR2 cell line was tumorigenic when injected *s.c.* in immunodeficient mice; tumors showed traits similar to patient's tumor sample (*Figure 3A* and Figure S2; for data of patient's tumor sample see *Patient clinical history and molecular data*). PD-L1 expression level on ADK-VR2 cells was homogeneous (Figure S3). In addition, ADK-VR2 showed high experimental metastatic ability since all mice receiving *i.v.* injection of these cells presented a high number of overt lung metastases (*Figure 3B,3C*). Crizotinib significantly reduced tumor growth although we did not observe a complete tumor regression (*Figure 3D*). We quantified the presence of spontaneous lung metastases, induced by *s.c.* injection of ADK-VR2,

by RT-PCR assay, and we detected the presence of human cells in lungs of mice enrolled in both control and crizotinib groups. Crizotinib reduced the metastatic load although this decrease did not reach statistical significance compared to the control group (*Figure 3E*).

Selection of a drug resistant variant

Clone AG143 was isolated from ADK-VR2 cells grown in 3D culture in the presence of crizotinib. According to Oncomine panel, ADK-VR2 AG143 cells maintained the same ROS1 translocation of the parental cells, with no other significant alteration. In adherent culture conditions, cells showed a polygonal morphology which was similar to the parental cell line one. ADK-VR2 AG143 clone had a significantly lower sensitivity to crizotinib than parental cell line in adherent cultures (IC_{50} >1.5 µM) (*Figure 4A*) and was not sensitive to lorlatinib, entrectinib and DS-6051b (Figure S4). Moreover, ADK-VR2 AG143 clone also showed a lower 3D-growth inhibition by crizotinib and DS-6051b than ADK-VR2. Interestingly, lorlatinib and DS-6051b resulted more effective than crizotinib on ADK-VR2 AG143 cell proliferation (*Figure 4B*).

The clone showed a lower ability to form spheres than parental cell line (ADK-VR2 AG143, number of spheres 95±7, n=4; ADK-VR2, number of spheres 164±7, n=4; P<0.001, by the Student's *t*-test). In addition, ADK-VR2 AG143 sphere formation (*Figure 4C*) was less affected by TKIs treatment than ADK-VR2 (*Figure 2E* and Table S3); lorlatinib (IC_{50} 3.2 nM) was more active than crizotinib (IC_{50} 23.6 nM), entrectinib (IC_{50} 59 nM) and DS-6051b (IC_{50} 106 nM) on ADK-VR2 AG143 sphere formation as well as on ADK-VR2.

In vivo growth of ADK-VR2 AG143 was slower than ADK-VR2, probably reflecting the lower stemness of these cells (*Figure 4D*). Tumors maintained histological and phenotypic traits similar to patient's tumor sample (*Figure 4E*, Figure S5; for patient's tumor sample see *Patient clinical history and molecular data*) and the expression of PD-L1 on ADK-VR2 AG143 cells was homogenous as well as for ADK-VR2 cells (Figure S3).

Discussion

ROS1 fusion-positive NSCLC accounts for 1–2% of NSCLC cases and the expression of fusion genes results in constitutive activation of ROS1-tyrosine kinase that drives malignant cell proliferation (28). Crizotinib is the current standard of care for patients with treatment-naïve advanced-stage ROS1 fusion-positive NSCLC. Novel generation TKIs such as lorlatinib and entrectinib have also been explored (3), the last receiving by EMA (EMA/303481/2020) a conditional marketing authorisation as monotherapy for the treatment of adult patients with ROS1-positive advanced NSCLC not previously treated with ROS1 inhibitors. In our case, at the time of progressive disease (including also brain) on platinum-based chemotherapy the best treatment choice included the use of one of these drugs; unfortunately, both ROS1 inhibitors were not available either in clinical trials or as compassionate use program.

The inevitable development of resistance in ROS1-positive NSCLCs treated with first-line TKIs remains a clinical challenge since little is known about the mechanisms of resistance and in particular *de-novo* resistance. The presence of *ROS1* point mutations or the activation of other RTKs seem to be involved in resistance. Anyway, the low frequency of *ROS1* fusion-positive tumors, the high number of *ROS1* partner genes and the scarce availability of preclinical models are limiting factors that hinder the understanding these mechanisms of drug resistance (3,28).

ADK-VR2 is a new cell line derived from the pleural effusion of a treatment-naïve NSCLC patient with *SDC4-ROS1* fusion that was primarily resistant to crizotinib. Although this alteration has been reported in NSCLC patients, to the best of our knowledge this is the first *in vitro* model directly derived from a tumor sample collected at the diagnosis and carrying this translocation, since similar preclinical models have not yet been obtained. Of note is the CUTO-2 cell line model described for the first time by Davies and colleagues (23), used to study the role of ROS1 fusion (10) and the mechanisms of crizotinib resistance (29,30). CUTO-2 cell line was the first model derived from a *SDC4-ROS1*-fusion positive NSCLC. Anyway, differently from ADK-VR2, CUTO-2 cell line was derived from the biopsy of a patient with an evidence of disease progression discovered approximately 18 weeks after the start of treatment. At that time, an excisional biopsy was performed, and CUTO-2 cell line was obtained (23). IC_{50} value of crizotinib on CUTO-2 cultured in 2D conditions was 0.38 µM (23), quite like ADK-VR2 cell line. Currently, HCC-78 cell line, bearing the *SLC34A2-ROS1* fusion, is the most used ROS1-rearranged NSCLC model for drug sensitivity tests (31-33). In the absence, several studies also used the transformed murine Ba/F3 interleukin-3 dependent pro-B cell line (34) expressing different ROS1 fusion genes

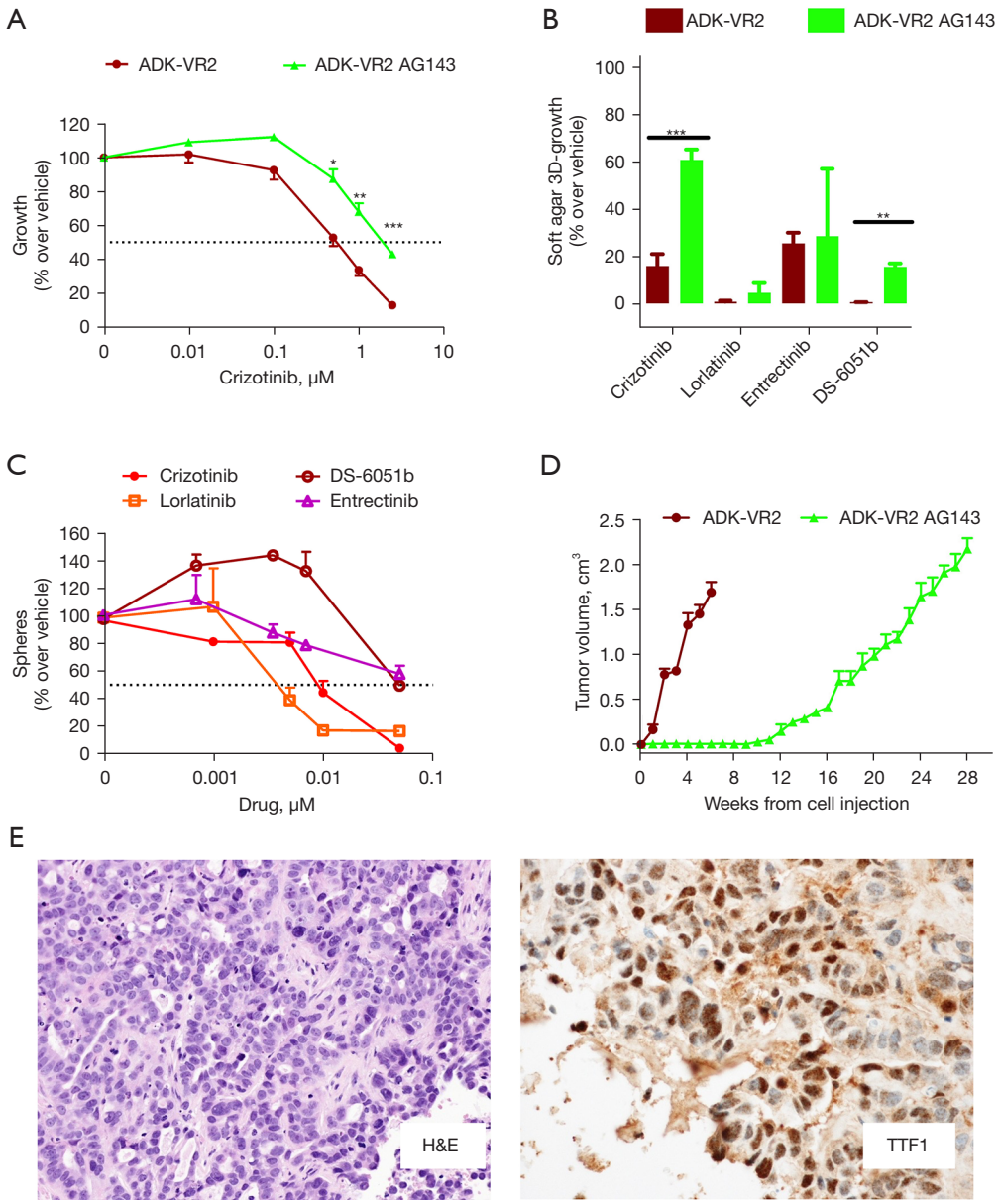

Figure 4 ADK-VR2 AG143 *in vitro* drug sensitivity (A-C) and *in vivo* growth (D,E). (A) ADK-VR2 (n=8, data also included in *Figure 2A*) and ADK-VR2 AG143 (n=2) sensitivity to crizotinib in 2D culture conditions. *, P<0.05; **, P<0.01; ***, P<0.001 by Student's *t*-test. Each point represents mean and SEM. (B) Soft agar 3D-growth of ADK-VR2 (data also included in *Figure 2D*) and ADK-VR2 AG143 in the presence of crizotinib 0.01 μM (n=4), lorlatinib 0.01 μM (n=4), entrectinib 0.01 μM (n=2) and DS-6051b 0.01 μM (n=2). ***, P<0.001; **, P<0.01 by Student's *t*-test. Each bar represents mean and SEM. (C) ADK-VR2 AG143 sphere formation (n=2) in the presence of crizotinib (IC_{50} 0.0236±0.0103 μM), lorlatinib (IC_{50} 0.0032±0.0012 μM), DS-6051b (IC_{50} 0.1060±0.0111 μM) and entrectinib (IC_{50} 0.0590±0.0110 μM) at different doses. Statistical significance by Student's *t*-test: P<0.05, lorlatinib *vs.* entrectinib and DS-6051b, crizotinib *vs.* DS-6051b. Each point represents mean and SEM. (D) Comparison of *in vivo* growth of ADK-VR2 and ADK-VR2 AG143 cells injected *s.c.* (9×10^6 cells) in immunocompromised BRG mice (n=3 for each group). Starting from 2nd week after cell injection, P<0.01 by unpaired *t*-test with Welch's correction. Each point represents mean and SEM. (E) Pictures representative of tumors induced by *s.c.* injection of ADK-VR2 AG143 cells in immunocompromised mice (×20 magnification). H&E stain showing a morphology similar to the tumor of the patient. TTF1 staining was weak and focal. H&E, hematoxylin and eosin; SEM, standard error of the mean; *s.c.*, subcutaneously; BRG, BALB/c *Rag2*$^{-/-}$;*Il2rg*$^{-/-}$; 2D, two-dimensional; 3D, three-dimensional.

to investigate TKI activity (3). In this context, ADK-VR2 cell line is a further promising model for studies on drug sensitivity in ROS1-rearranged tumors, considering its tumorigenic ability and its tendency to develop spontaneous and induced lung metastases.

Our study demonstrated that ADK-VR2 cells are less sensitive to pemetrexed than HCC-78 cell line, which is considered to be sensitive to this drug (23) as most ROS1-positive NSCLC cell lines. This experimental result is consistent with the clinical outcome in our patient who displayed unexpected chemotherapy-resistance. On the other hand, the two cell lines showed a similar 2D-growth behaviour in the presence of crizotinib. The activity of crizotinib on ADK-VR2 cells was also confirmed *in vivo*, since the drug was able to effectively control ADK-VR2 tumor growth. Nevertheless, tumor was not completely cured and metastatic cells were also detected in lungs. This result partially mirrored the poor activity of the drug observed in the patient who did not benefit from crizotinib, probably due to the high tumor volume and a broad clonal heterogeneity. Of note, lorlatinib, which did not show any inhibitory activity in 2D tests, resulted to be able to inhibit ADK-VR2 3D-growth and sphere formation. Similarly, other authors reported that crizotinib-resistant HCC-78 cells can show drug re-sensitization in 3D conditions since the non-attachment culture conditions restore the ROS1 oncogene dependence of cells by suppressing the EGFR feedback pathway (35). For what concerns entrectinib and DS-6051b, these drugs were not active in 2D tests and showed a lower activity compared to lorlatinib in sphere formation inhibition. Overall, in this model we observed a modulation of drug sensitivity depending on culture conditions, which may be representative of different tumor microenvironment conditions. In this context, drugs that are more active in 3D culture or stem cell-selective conditions may be more effective in counteracting initial metastatic dissemination and growth when cells are not sustained by other microenvironment elements.

Furthermore, ADK-VR2 AG143 clone, grown in 3D cell culture in the presence of crizotinib, was more resistant to crizotinib than the parental cell line, both in 2D and 3D/sphere formation tests, while maintaining the same sensitivity to lorlatinib. However, ADK-VR2 AG143 Oncomine analysis did not reveal the presence of additional molecular alterations compared to the parental cell line ADK-VR2 ones. In addition, we also observed a lower sphere-formation ability and slower *in vivo* growth than ADK-VR2 cells. It is well known that cancer stem cells play a critical role in tumor aggressiveness and TKI resistance (36). Recently, Dias and Bernards suggested a new therapeutic approach based on the overactivation of mitogenic signals to disrupt the labile homeostasis of cancer cells and overload stress response pathways in advanced cancers resistant to target therapy (37). In addition, crizotinib has been reported to negatively correlate with the ALK-dependent transcription of noncoding RNAs (ncRNAs) implicated in the maintenance of stemness properties in *EML-ALK*$^{+}$ NSCLC cell cultures (38). Since ROS1 and ALK activate the same signaling pathways (39), ROS1 may be responsible for ncRNAs transcription that may be lost in the AG143 clone, since grown in the presence of crizotinib. Further studies are needed to confirm these hypotheses and to investigate the currently unknown mechanisms of resistance to crizotinib in ADK-VR2 AG143 cell line. Single cell DNA and RNA sequencing will give us the chance to identify distinct cell populations. Furthermore, WES analysis of the clone AG143 and its comparison to the parental ADK-VR2 cells will add new information regarding the mechanisms of crizotinib resistance.

Conclusions

In conclusion, we propose ADK-VR2 cell line as a new preclinical model to study novel and more effective anti-cancer drugs for ROS1-positive NSCLC. The advantage of working with cells that have not gone through a previous selection process because of in-patient treatment, together with the ability of cells to grow and metastasize *in vivo*, makes this cell line a very promising and useful model for both the study of the functional role of the fused SDC4-ROS1 gene and the study of new targeted drugs for the treatment of NSCLCs, or other carcinomas and sarcomas, carrying this ROS1 fusion.

Acknowledgments

The authors would thank Prof. Andrea Cavazzoni (from Department of Medicine and Surgery, University of Parma, Parma, Italy) for the critical reading of the manuscript and his suggestions and Prof. Maria Pantaleo (from Department of Experimental, Diagnostic and Specialty Medicine, University of Bologna, Bologna, Italy) for the use of whole exome sequencing platform.

Funding: This work was supported by Ricerca Finalizzata Ministero della Salute 2018 grant, number GR-2018-12368031 (to Francesco Gelsomino, Arianna Palladini);

the Department of Experimental, Diagnostic and Specialty Medicine of the University of Bologna ("Pallotti" Fund to Pier-Luigi Lollini, Patrizia Nanni); the University of Bologna, Fundamentally Oriented Research funds (to Pier-Luigi Lollini, Patrizia Nanni, Arianna Palladini); CARISBO Foundation, grant 2019-0543 (to Pier-Luigi Lollini); AIRC IG (ID 25789 project to Manuela Ferracin).

Footnote

Reporting Checklist: The authors have completed the ARRIVE reporting checklist. Available at https://tlcr.amegroups.com/article/view/10.21037/tlcr-22-163/rc

Data Sharing Statement: Available at https://tlcr.amegroups.com/article/view/10.21037/tlcr-22-163/dss

Peer Review File: Available at https://tlcr.amegroups.com/article/view/10.21037/tlcr-22-163/prf

Conflicts of Interest: All authors have completed the ICMJE uniform disclosure form (available at https://tlcr.amegroups.com/article/view/10.21037/tlcr-22-163/coif). Andrea Ardizzoni received grants and personal fees from Bristol-Myers Squibb, Merck Sharp & Dohme, Eli Lilly, Boehringer Ingelheim and Pfizer, grants from Celgene and grants and personal fees from Roche, outside of the submitted work. FG received grants from Astrazeneca and honoraria for advisory board participation from Eli-Lilly. The other authors declare no conflicts of interest.

Ethical Statement: The authors are accountable for all aspects of the work in ensuring that questions related to the accuracy or integrity of any part of the work are appropriately investigated and resolved. All animal procedures were performed in accordance with European directive 2010/63/UE and Italian Law (No. DL26/2014); experimental protocols were reviewed and approved by the institutional animal care and use committee of the University of Bologna and by the Italian Ministry of Health with letter 32/2020-PR. The study was conducted in accordance with the Declaration of Helsinki (as revised in 2013). Human samples were collected after patient gave his informed consent. The protocol was approved by the Ethics Committee Center Emilia-Romagna Region, Italy (protocol 130/2016/U/Tess). Human samples and metadata including relevant clinical data were de-identified before being shared between laboratories involved in this study.

References

1. Gridelli C, Rossi A, Carbone DP, et al. Non-small-cell lung cancer. Nat Rev Dis Primers 2015;1:15009.
2. Rotow J, Bivona TG. Understanding and targeting resistance mechanisms in NSCLC. Nat Rev Cancer 2017;17:637-58.
3. Drilon A, Jenkins C, Iyer S, et al. ROS1-dependent cancers – biology, diagnostics and therapeutics. Nat Rev Clin Oncol 2021;18:35-55.
4. Robinson DR, Wu YM, Lin SF. The protein tyrosine kinase family of the human genome. Oncogene 2000;19:5548-57.
5. Kiyozumi D, Noda T, Yamaguchi R, et al. NELL2-mediated lumicrine signaling through OVCH2 is required for male fertility. Science 2020;368:1132-5.
6. Suehara Y, Kohsaka S, Hayashi T, et al. Identification of a Novel MAN1A1-ROS1 Fusion Gene Through mRNA-based Screening for Tyrosine Kinase Gene Aberrations in a Patient with Leiomyosarcoma. Clin Orthop Relat Res 2021;479:838-52.
7. Comandini D, Catalano F, Grassi M, et al. Outstanding Response in a Patient With ROS1-Rearranged Inflammatory Myofibroblastic Tumor of Soft Tissues Treated With Crizotinib: Case Report. Front Oncol 2021;11:658327.
8. Ou SI, Nagasaka M. A Catalog of 5' Fusion Partners in ROS1-Positive NSCLC Circa 2020. JTO Clin Res Rep 2020;1:100048.
9. Li Z, Shen L, Ding D, et al. Efficacy of Crizotinib among Different Types of ROS1 Fusion Partners in Patients with ROS1-Rearranged Non-Small Cell Lung Cancer. J Thorac Oncol 2018;13:987-95.
10. Neel DS, Allegakoen DV, Olivas V, et al. Differential Subcellular Localization Regulates Oncogenic Signaling by ROS1 Kinase Fusion Proteins. Cancer Res 2019;79:546-56.
11. Park S, Ahn BC, Lim SW, et al. Characteristics and

Outcome of ROS1-Positive Non-Small Cell Lung Cancer Patients in Routine Clinical Practice. J Thorac Oncol 2018;13:1373-82.
12. Chen YF, Hsieh MS, Wu SG, et al. Efficacy of Pemetrexed-Based Chemotherapy in Patients with ROS1 Fusion-Positive Lung Adenocarcinoma Compared with in Patients Harboring Other Driver Mutations in East Asian Populations. J Thorac Oncol 2016;11:1140-52.
13. Song Z, Su H, Zhang Y. Patients with ROS1 rearrangement-positive non-small-cell lung cancer benefit from pemetrexed-based chemotherapy. Cancer Med 2016;5:2688-93.
14. Shaw AT, Ou SH, Bang YJ, et al. Crizotinib in ROS1-rearranged non-small-cell lung cancer. N Engl J Med 2014;371:1963-71.
15. Nokin MJ, Ambrogio C, Nadal E, et al. Targeting Infrequent Driver Alterations in Non-Small Cell Lung Cancer. Trends Cancer 2021;7:410-29.
16. Nomura T, Tamaoki N, Takakura A, et al. Basic concept of development and practical application of animal models for human diseases. Curr Top Microbiol Immunol 2008;324:1-24.
17. Palladini A, Thrane S, Janitzek CM, et al. Virus-like particle display of HER2 induces potent anti-cancer responses. Oncoimmunology 2018;7:e1408749.
18. Palladini A, Nicoletti G, Lamolinara A, et al. HER2 isoforms co-expression differently tunes mammary tumor phenotypes affecting onset, vasculature and therapeutic response. Oncotarget 2017;8:54444-58.
19. Giusti V, Ruzzi F, Landuzzi L, et al. Evolution of HER2-positive mammary carcinoma: HER2 loss reveals claudin-low traits in cancer progression. Oncogenesis 2021;10:77.
20. Nanni P, Nicoletti G, Palladini A, et al. Multiorgan metastasis of human HER-2+ breast cancer in Rag2-/-;Il2rg-/- mice and treatment with PI3K inhibitor. PloS One 2012;7:e39626.
21. Landuzzi L, Palladini A, Ceccarelli C, et al. Early stability and late random tumor progression of a HER2-positive primary breast cancer patient-derived xenograft. Sci Rep 2021;11:1563.
22. Eisenhauer EA, Therasse P, Bogaerts J, et al. New response evaluation criteria in solid tumours: revised RECIST guideline (version 1.1). Eur J Cancer 2009;45:228-47.
23. Davies KD, Mahale S, Astling DP, et al. Resistance to ROS1 inhibition mediated by EGFR pathway activation in non-small cell lung cancer. PloS One 2013;8:e82236.
24. Sun L, Han T, Zhang X, et al. PRRX1 isoform PRRX1A regulates the stemness phenotype and epithelial-mesenchymal transition (EMT) of cancer stem-like cells (CSCs) derived from non-small cell lung cancer (NSCLC). Transl Lung Cancer Res 2020;9:731-44.
25. Tung CH, Huang MF, Liang CH, et al. α-Catulin promotes cancer stemness by antagonizing WWP1-mediated KLF5 degradation in lung cancer. Theranostics 2022;12:1173-86.
26. Dimitrakopoulos FD, Kottorou AE, Kalofonou M, et al. The Fire Within: NF-κB Involvement in Non-Small Cell Lung Cancer. Cancer Res 2020;80:4025-36.
27. Parakh S, Ernst M, Poh AR. Multicellular Effects of STAT3 in Non-small Cell Lung Cancer: Mechanistic Insights and Therapeutic Opportunities. Cancers (Basel) 2021;13:6228.
28. Azelby CM, Sakamoto MR, Bowles DW. ROS1 Targeted Therapies: Current Status. Curr Oncol Rep 2021;23:94.
29. Dziadziuszko R, Le AT, Wrona A, et al. An Activating KIT Mutation Induces Crizotinib Resistance in ROS1-Positive Lung Cancer. J Thorac Oncol 2016;11:1273-81.
30. Pilling AB, Kim J, Estrada-Bernal A, et al. ALK is a critical regulator of the MYC-signaling axis in ALK positive lung cancer. Oncotarget 2018;9:8823-35.
31. Bergethon K, Shaw AT, Ou SH, et al. ROS1 rearrangements define a unique molecular class of lung cancers. J Clin Oncol 2012;30:863-70.
32. Davies KD, Le AT, Theodoro MF, et al. Identifying and targeting ROS1 gene fusions in non-small cell lung cancer. Clin Cancer Res 2012;18:4570-9.
33. Yasuda H, de Figueiredo-Pontes LL, Kobayashi S, et al. Preclinical rationale for use of the clinically available multitargeted tyrosine kinase inhibitor crizotinib in ROS1-translocated lung cancer. J Thorac Oncol 2012;7:1086-90.
34. Warmuth M, Kim S, Gu XJ, et al. Ba/F3 cells and their use in kinase drug discovery. Curr Opin Oncol 2007;19:55-60.
35. Gong B, Oh-Hara T, Fujita N, et al. 3D culture system containing gellan gum restores oncogene dependence in ROS1 rearrangements non-small cell lung cancer. Biochem Biophys Res Commun 2018;501:527-33.
36. Del Re M, Arrigoni E, Restante G, et al. Concise Review: Resistance to Tyrosine Kinase Inhibitors in Non-Small Cell Lung Cancer: The Role of Cancer Stem Cells. Stem Cells 2018;36:633-40.
37. Dias MH, Bernards R. Playing cancer at its own game: activating mitogenic signaling as a paradoxical intervention. Mol Oncol 2021;15:1975-85.
38. Yang Y, Huang J, Xie N, et al. lincROR influences the stemness and crizotinib resistance in EML-ALK+

non-small-cell lung cancer cells. Onco Targets Ther 2018;11:3649-57.
39. Chevallier M, Borgeaud M, Addeo A, et al. Oncogenic driver mutations in non-small cell lung cancer: Past, present and future. World J Clin Oncol 2021;12:217-37.

Cite this article as: Ruzzi F, Angelicola S, Landuzzi L, Nironi E, Semprini MS, Scalambra L, Altimari A, Gruppioni E, Fiorentino M, Giunchi F, Ferracin M, Astolfi A, Indio V, Ardizzoni A, Gelsomino F, Nanni P, Lollini PL, Palladini A. ADK-VR2, a cell line derived from a treatment-naïve patient with *SDC4-ROS1* fusion-positive primarily crizotinib-resistant NSCLC: a novel preclinical model for new drug development of ROS1-rearranged NSCLC. Transl Lung Cancer Res 2022;11(11):2216-2229. doi: 10.21037/tlcr-22-163

Appendix 1

Methods

NGS

For the Next Generation Sequencing (NGS), slides were manually macrodissected, and the RNA was isolated. Library were prepared by the Oncomine Focus Assay (Thermo Fisher Scientific) using a total of 10 ng input RNA per sample. The RNA panel can identify rearrangements in 23 genes including ROS1. Sequencing was performed using the Ion GeneStudio S5 (Thermo Fisher Scientific). Fusions were detected using the fusion detection module within the Ion Reporter workflow, in particular 20,000 was the minimum number of total valid mapped reads required to qualify a sample as valid and to proceed with the analysis.

FISH

The break-apart FISH test is based on a mixture of two probes hybridizing to the proximal (3', green-labeled probe) and distal (5', orange-labeled probe) to the ROS1 breakpoint cluster region. At least 50 non-overlapping tumor nuclei were scored for each specimen by a trained technologist and a pathologist. Cells positive for rearrangement were defined by two main patterns: i) a "split pattern", with 3' and 5' break apart signals at a distance of two times the diameter of the largest signal; ii) a "5' deletion pattern", showing one fusion signal and an isolated 3'green signal (without the corresponding 5' orange signal). A case was considered FISH positive for ROS1 rearrangements when at least 15% of tumor cells showed any split or any 5' deletion pattern.

Whole Transcriptome Sequencing and Whole Exome Sequencing

For Whole Transcriptome Sequencing (WTS), poly(A)-RNA molecules were purified using oligo-dT magnetic beads, then mRNA was fragmented and randomly primed for reverse transcription, followed by second-strand synthesis. The cDNA fragments were end-repaired, ligated using paired-end sequencing adapters and amplified to create the final cDNA library.

For Whole Exome Sequencing (WES), genomic DNA was tagged and fragmented by the Nextera transposon-based technique, then DNA libraries were denatured to single-stranded DNA and hybridized to biotin-labeled 80-mer probes designed to enrich targeted exonic regions, then eluted from magnetic beads and amplified by PCR.

WTS and WES libraries were quality checked and sized with the High Sensitivity kit on the 2100 Bioanalyzer (Agilent Technologies), then quantified using a fluorometric assay (Quant-iT PicoGreen Assay, Life Technologies). Paired-end libraries were sequenced at 2 × 80 bp read length on a Nextseq500 Illumina platform.

NGS data analysis of WES was performed as follows. After cleaning and trimming (https://adapterremoval.readthedocs.io), paired-end reads (80X2) were aligned to human reference HG38 using the Burrows-Wheeler Aligner (http://bio-bwa.sourceforge.net/), bam file manipulation including PCR duplicates removal were performed using Samtools (http://www.htslib.org/). Mapping quality recalibration and local realignment around indels was performed using Genome Analysis Toolkit (GATK4) as well as the detection of single nucleotide variants (SNVs) and indels (function mutect2) (https://gatk.broadinstitute.org). All detected variants were filtered based on quality, coverage >15X, allele ratio >0.2, and the presence in public databases (dbSNP and Exac). Somatic mutations were called by comparing with normal counterpart sample. Functional annotation was performed with Annovar tool (http://www.openbioinformatics.org/annovar/). Differently, WTS data was analyzed with the aim to detect chimeric transcripts adopting a consensus method based on both Chimerascan (https://code.google.com/archive/p/chimerascan/) and Defuse (https://github.com/amcpherson/defuse) algorithms.

Flow Cytometry analysis

PD-L1 detection on ADK-VR2, ADK-VR2 AG143 and HCC-78 was performed by indirect direct immunofluorescence with 5 µg/mL anti-PD-L1 antibody (Tecentriq1200, atezolizumab, Roche). Anti-mouse IgGAF488 (diluted 1:100; Thermo Fisher Scientific) was used as secondary antibody. Cytofluorometric analysis was performed by CyFlow Space (Sysmex Partec, Germany) instrument and analyzed using FCSExpress (De Novo Software, Glendale, CA, USA).

https://dx.doi.org/10.21037/tlcr-22-163

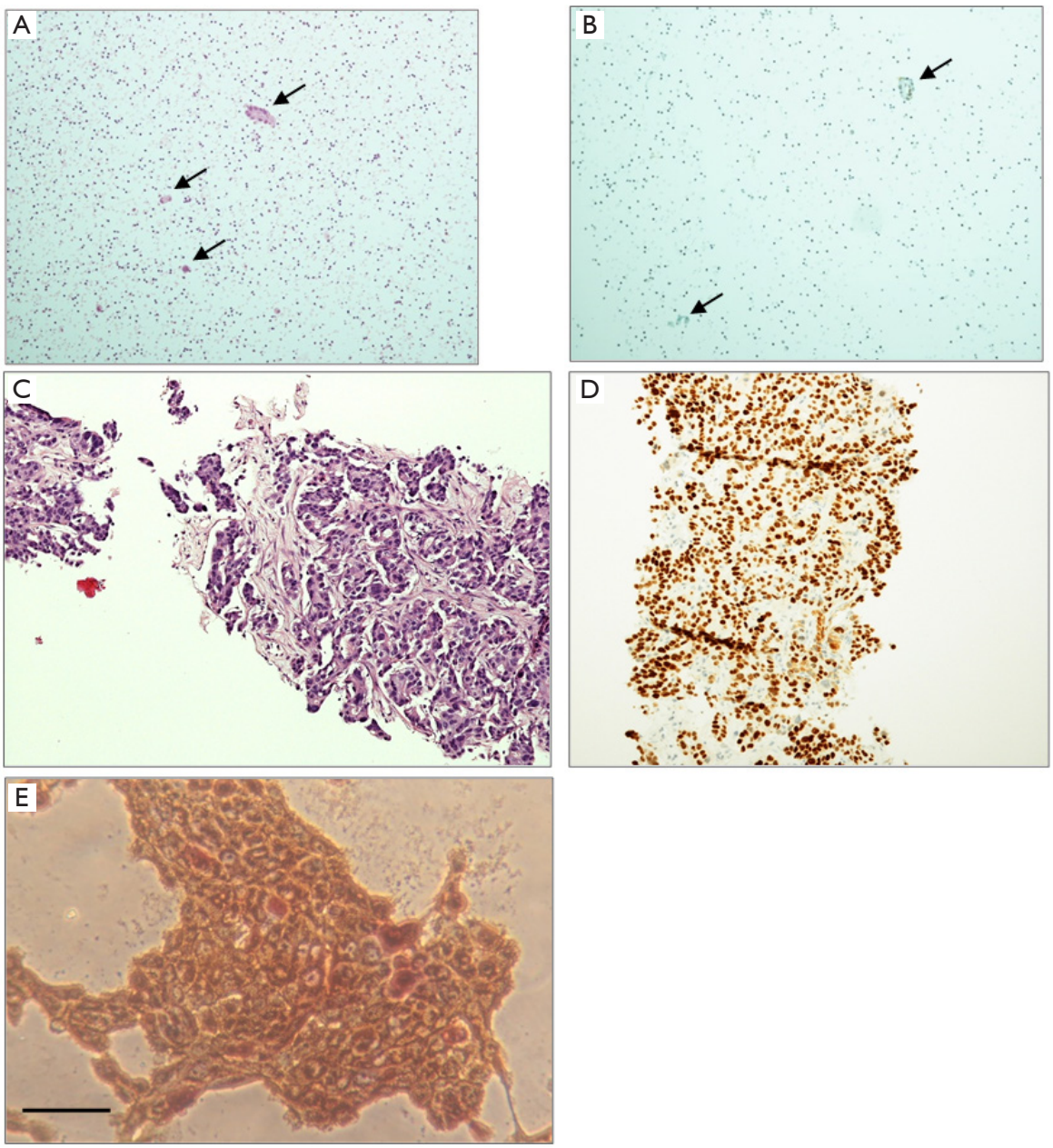

Figure S1 Molecular and morphological characterization of patient's tumor samples and ADK-VR2 cell line. (A,B) Cytological cell blocks from malignant pleural effusion of the patient at the diagnosis. (A) H&E staining showing aggregates of neoplastic cells (arrows) ×10 magnification. (B) TTF1 staining evidencing a focal positivity (arrows) ×10 magnification. (C,D) Liver metastasis. (C) H&E staining. (D) TTF1 staining. (E) BerEP4 staining of ADK-VR2 cell line. Black bar corresponds to 100 µm. H&E, hematoxylin and eosin.

https://dx.doi.org/10.21037/tlcr-22-163

Table S1 Somatic mutations evidenced in ADK-VR2 cells by whole exome sequencing

Gene symbol	NCBI transcript ID	Exon	cDNA variant	Protein variant	Depth of coverage[†]	Allele frequency[‡]
ANK2	NM_001148	exon38	c.C8837A	p.T2946K	220	0.655
CNTNAP5	NM_130773	exon22	c.G3542A	p.R1181H	30	0.367
COX11	NM_001162862	exon1	c.G53T	p.R18L	149	0.517
CSMD1	NM_033225	exon37	c.G5635A	p.A1879T	32	0.625
CWF19L1	NM_001303406	exon4	c.C263T	p.A88V	113	0.239
DEFA6	NM_001926	exon1	c.G130T	p.A44S	89	0.674
DIS3	NM_001128226	exon16	c.C1975G	p.R659G	22	1.000
FGA	NM_000508	exon6	c.G2574A	p.M858I	114	0.377
GNA14	NM_004297	exon1	c.G25A	p.A9T	82	1.000
JKAMP	NM_001284201	exon5	c.A659C	p.Q220P	32	1.000
LOXL2	NM_002318	exon14	c.G2246A	p.G749D	60	0.267
LRP6	NM_002336	exon4	c.A809G	p.D270G	212	0.476
MEI1	NM_152513	exon13	c.G1453A	p.A485T	22	1.000
NUP98	NM_016320	exon29	c.A4492C	p.I1498L	65	1.000
PANX3	NM_052959	exon1	c.G163A	p.A55T	112	0.580
PKD1L1	NM_138295	exon9	c.A1402C	p.S468R	37	0.649
PKHD1	NM_138694	exon41	c.G6698C	p.G2233A	150	0.367
PLB1	NM_001170585	exon57	c.T4219G	p.W1407G	96	0.677
TTC36	NM_001080441	exon3	c.G388A	p.G130R	164	0.396
TTK	NM_001166691	exon17	c.C2044T	p.Q682X	30	0.500
ZBTB24	NM_001164313	exon2	c.G157A	p.A53T	93	0.473
ZNF285	NM_001291489	exon4	c.G809T	p.S270I	159	0.358
DMKN	NM_001190348	exon1	c.G159C	p.K53N	250	0.468

[†], depth of coverage refers to the total number of short reads overlapping the given genomic coordinate in which the mutation was found; [‡], allele frequency refers to the ratio between the number of short reads carrying the mutated allele and the depth of coverage.

Table S2 Drug sensitivity on 2D cultures in ADK-VR2, HCC-78 and clone AG143 to various drugs

Cell line	Pemetrexed (μM)	Crizotinib (μM)	Lorlatinib (μM)	Entrectinib (μM)	DS-6051b (μM)
ADK-VR2	0.0677±0.0130	0.5530±0.0801	>2.5	>1	>1
ADK-VR2 AG143	–	1.5500±0.1463	>2.5	>1	>1
HCC-78	0.0096±0.0009	0.4686±0.2494	<0.01	0.2967±0.1182	0.4309±0.2459

IC_{50} mean ± SEM was reported. SEM, standard error of mean.

Table S3 Drug sensitivity on sphere formation assay in ADK-VR2 and clone AG143 to various drugs

Cell line	Crizotinib (μM)	Lorlatinib (μM)	Entrectinib (μM)	DS-6051b (μM)
ADK-VR2	0.0040±0.0003	0.0003±0.0001	0.0233±0.0049	0.0013±0.0000
ADK-VR2 AG143	0.0236±0.0103	0.0032±0.0012	0.0590±0.0110	0.1060±0.0111

IC_{50} mean ± SEM was reported. SEM, standard error of mean.

https://dx.doi.org/10.21037/tlcr-22-163

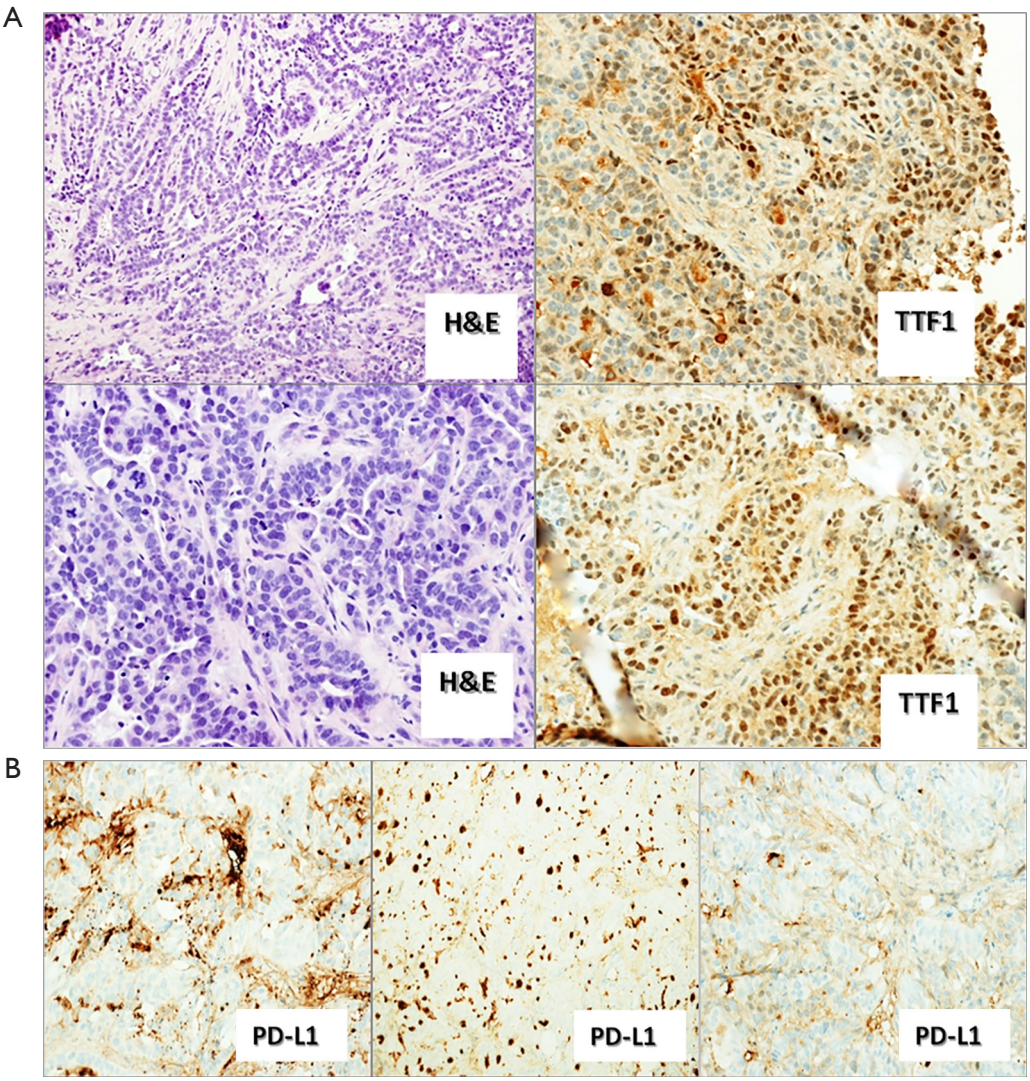

Figure S2 Tumors induced by s.c. injection of ADK-VR2 cells in immunocompromised BRG mice. (A) The phenotype of tumors developed in three different mice was studied. Each row represents a distinct tumor. H&E showed a morphology similar to tumor of patient. TTF1 staining was focal. The third tumor was reported in *Figure 3A* (×10 magnification). (B) PD-L1 staining of three different tumors was weak and focal for the first and second tumor and negative for the third tumor (×10 magnification).

https://dx.doi.org/10.21037/tlcr-22-163

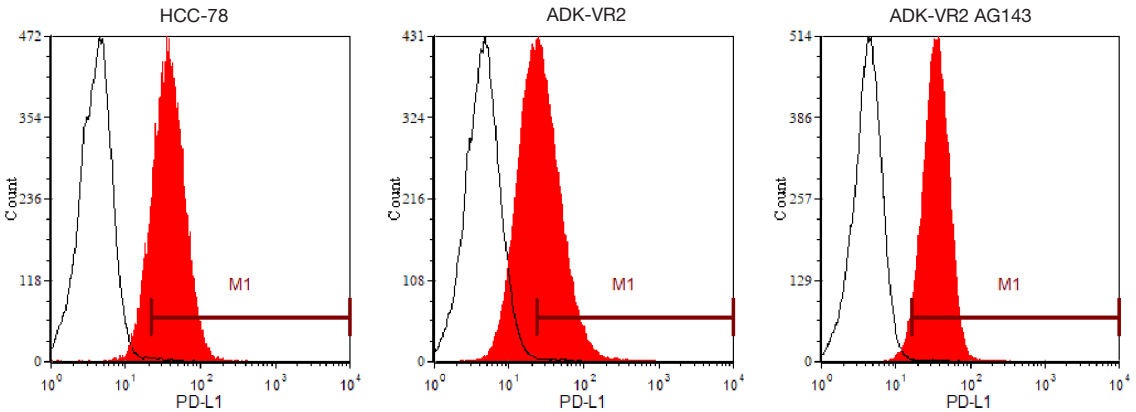

Figure S3 Panels show representative profiles of PD-L1 level expressed on HCC-78, ADK-VR2 and ADK-VR2 AG143 as measured by flow cytometry. Black profile, secondary antibody alone; red profile, anti-PD-L1 antibody.

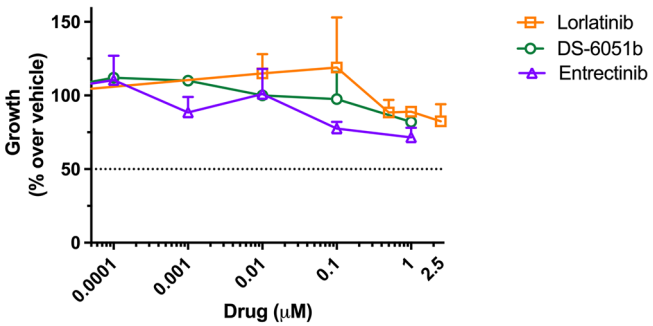

Figure S4 *In vitro* 2D-growth sensitivity of ADK-VR2 AG143 cells to lorlatinib (n=2), DS-6051b (n=2) and entrectinib (n=2). Each point represents mean and SEM. SEM, standard error of mean.

https://dx.doi.org/10.21037/tlcr-22-163

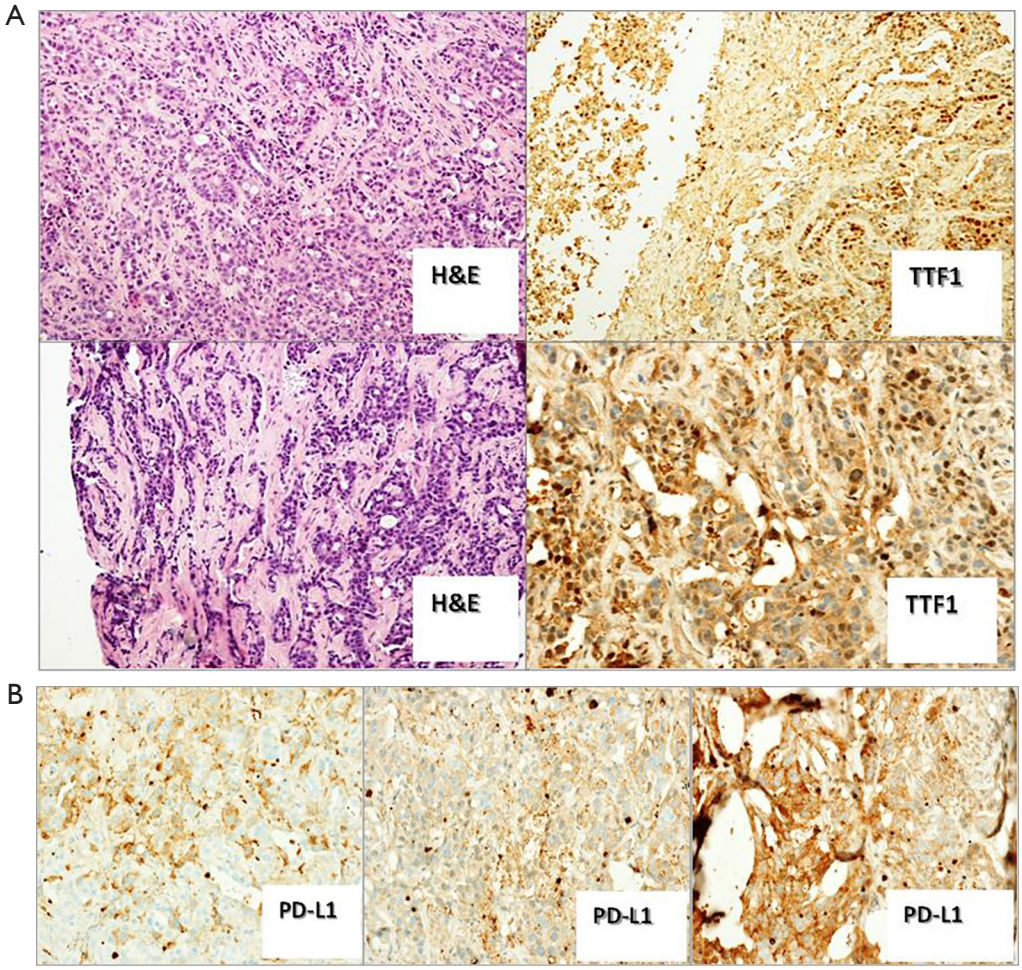

Figure S5 Tumors induced by s.c. injection of ADK-VR2 AG143 cells in immunocompromised BRG mice. (A) The phenotype of tumors developed in three different mice was studied. The picture depicted the tumors of two mice. The third one was included in *Figure 4*. Each row represents a distinct tumor. First column: H&E staining showing a morphology similar to the tumor of the patient. Second column: weak and focal TTF1 staining (×10 magnification). (B) PD-L1 staining of three distinct ADK-VR2 AG143 tumors: the expression was weak and focal for the first and second tumor and negative for the third tumor (×10 magnification). H&E, hematoxylin and eosin.

https://dx.doi.org/10.21037/tlcr-22-163